Vertical characterization of Highly Oxygenated Molecules (HOMs) below and above a boreal forest canopy

Qiaozhi Zha[1], Chao Yan[1], Heikki Junninen[1], Matthieu Riva[1], Nina Sarnela[1], Juho Aalto[1], Lauriane Quéléver[1], Simon Schallhart[1], Lubna Dada[1], Liine Heikkinen[1], Otso Peräkylä[1], Jun Zou[2], Clémence Rose[1], Yonghong Wang[1], Ivan Mammarella[3], Gabriel Katul[4,5], Timo Vesala[1], Douglas R. Worsnop[1,6], Markku Kulmala[1], Tuukka. Petäjä[1], Federico Bianchi[1], and Mikael Ehn[1]

[1] Institute for Atmospheric and Earth System Research/Physics, Faculty of Science, University of Helsinki, P.O. Box 64, 00014 Helsinki, Finland
[2] CMA-NJU Joint Laboratory for Climate Prediction Studies, Institute for Climate and Global Change Research, School of Atmospheric Sciences, Nanjing University, Nanjing, China
[3] Department of Physics, University of Helsinki, P.O. Box 48, 00014 Finland
[4] Nicholas School of the Environment, Duke University, Durham, North Carolina, USA
[5] Department of Civil and Environmental Engineering, Duke University, Durham, North Carolina, USA
[6] Aerodyne Research, Inc., Billerica, MA 01821, USA

1 Abstract

While the role of highly oxygenated molecules (HOMs) in new particle formation (NPF) and secondary organic aerosol (SOA) formation is not in dispute, the interplay between HOM chemistry and atmospheric conditions continues to draw significant research attention. During the Influence of Biosphere-Atmosphere Interactions on the Reactive Nitrogen budget (IBAIRN) campaign, profile measurements of neutral HOM molecules below and above the forest canopy were performed for the first time in the boreal forest SMEAR II station during September 2016. The HOM concentrations and composition distributions below and above the canopy were similar, supporting a well-mixed boundary layer approximation during daytime. However, much lower HOM concentrations were frequently observed at ground level, which was likely due to the

formation of a shallow decoupled layer below the canopy. Near ground HOMs were influenced by the changes in the precursors and oxidants, and enhancement of the loss on surfaces in this layer, while the HOMs above the canopy top were not significantly affected. Our findings also illustrate that near-ground HOM measurements conducted in strong stably stratified conditions at this site might only be representative of a small fraction of the entire nocturnal boundary layer. This could, in turn, influence the growth of newly formed particles and SOA formation below the canopy where a large majority of measurements are typically conducted.

2 Introduction

Highly oxygenated molecules (HOMs), a sub-group of the oxidation products of volatile organic compounds (VOCs) identified by their high oxidation states, have been recognized as important precursors for organic aerosol in the atmosphere (Ehn et al., 2014). They have also been found to enhance new particle formation (NPF) and growth (Kulmala et al., 2013; Zhao et al., 2013; Ehn et al., 2014; Bianchi et al., 2016; Kirkby et al., 2016; Tröstl et al., 2016). The importance of HOMs has been confirmed in ambient environments, especially in monoterpene-dominated regions such as the boreal forest (Kulmala et al., 2013; Ehn et al., 2014), but also in high altitude mountain regions (Bianchi et al., 2016) and in rural areas (Jokinen et al., 2014; Kürten et al., 2016). In laboratory studies, HOM formation has been observed from various precursor molecules (Ehn et al., 2017), including both biogenic and anthropogenic emissions.

The direct observation of HOMs has only recently become possible, following the developments of the Atmospheric-Pressure-interface Time-Of-Flight (APi-TOF, measures the charged HOM clusters) (Junninen et al., 2010) and Chemical Ionization Atmospheric-Pressure-interface Time-Of-Flight (CI-APi-TOF, measures the neutral HOM molecules) (Jokinen et al., 2012) mass spectrometers. Ehn et al. (2010) and Bianchi et al. (2017) found that the naturally charged HOM clusters could be observed

every night in boreal forest during spring. Out of the observed ambient mass spectra, a significant part could be reproduced in a chamber by introducing the monoterpene α-pinene ($C_{10}H_{16}$, the major biogenic VOC in the boreal forest) and ozone (O_3) (Ehn et al., 2012).

Further investigations of HOM formation chemistry have been done in both laboratory and field studies. Based on current understanding from laboratory experiments, the formation of HOM molecules involves three main steps: 1) initial formation of peroxy radicals (RO_2) from VOC oxidation; 2) RO_2 auto-oxidation, that is, the isomerization of the RO_2 via intramolecular H-shifts and the subsequent oxygen (O_2) additions; and 3) radical termination, forming closed-shell molecules (Crounse et al., 2013; Ehn et al., 2014; Jokinen et al., 2014, 2016; Rissanen et al., 2014; Mentel et al., 2015). In the atmosphere, HOM formation studies are complicated by the plethora of different compounds and processes taking place. However, recent ambient measurements together with factor analysis were able to shed light on the HOM formation pathways in the boreal forest (Yan et al., 2016). They showed that the majority of the daytime production of HOMs was from reactions initiated by the oxidation of monoterpenes (MT) with hydroxyl radical (OH) or O_3. The RO_2 after auto-oxidation was either terminated by hydroperoxyl radical (HO_2) or self-termination (Orlando and Tyndall, 2012), to form a non-nitrate HOM monomer ($CHO_{monomer}$, mainly C_9 and C_{10} compounds, with masses between 290-450 Th after clustering with the charging ion (NO_3^-) of the instrument); or reacting with nitrogen oxides (NO_x) to form an organonitrate HOM monomer ($CHON_{monomer}$). During nighttime, MT were mainly oxidized by O_3 and NO_3 radical. Furthermore, due to the lower nocturnal HO_2 and NO_x concentrations, besides the production of $CHON_{monomer}$, the RO_2 products could also react with another RO_2 to form a non-nitrate HOM dimer (CHO_{dimer}, mainly $C_{16\text{-}20}$ compounds, with masses between 450-600 Th after clustering with NO_3^-) or an organonitrate HOM dimer ($CHON_{dimer}$), depending on the oxidants of the RO_2 radical.

(Ehn et al., 2014; Jokinen et al., 2014; Yan et al., 2016; Berndt et al., 2018).

Beyond those chemical pathways, varied meteorological conditions are also factors influencing the MT and oxidants at different heights above the forest floor. Unsurprisingly, the oxidants producing HOMs (e.g. O_3) were found almost uniformly distributed within the well-mixed daytime boundary layer (Chen et al., 2018). In contrast, the nocturnal boundary layer was shallow with stability regimes that depended on radiative cooling within the canopy and turbulent shear stresses at the canopy top. In Hyytiälä, the depletions of O_3 below the canopy were frequently observed during nighttime, while the O_3 above the canopy was less affected. The MT concentration at ground level increased when O_3 was depleted (Eerdekens et al., 2009). The inhomogeneous distribution of the precursors and oxidants below and above the canopy might further impact nocturnal HOM distributions, which frames the scope of this study. Until now, all CI-APi-TOF deployments have been at ground level, and the main subject of inquiry here is the vertical information on HOMs and the role of meteorological condition in shaping them. A characterization of the HOMs at different heights provides a decisive advantage in disentangling the role of non-uniform mixing within the atmospheric layers impacted by strong thermal stratification, especially inside the canopy volume.

The first measurements of the HOM concentrations at two different heights (36 m and 1.5 m a.g.l.) during September 2016 are presented and discussed. The influence of boundary layer dynamics on the HOMs at these different heights at SMEAR II station are analyzed and characterized in conjunction with auxiliary turbulence and micrometeorological measurements.

3 Experimental

3.1 Measurement site description

The measurements were performed at the SMEAR II station (Station for Measuring Ecosystem–Atmosphere Relations) in the boreal forest in Hyytiälä, southern Finland (61°51' N, 24°17' E, 181 m a.s.l., Hari and Kulmala, 2005; Hari et al., 2013) during September 2016. There is no large anthropogenic emission source at or near the site. The closest sources are the two sawmills ~5 km southeast of the site, and from the city area of Tampere (~60 km away). The forest surrounding the station is primarily Scots pine with a mean canopy height of ~17.5 m, a total leaf area index (LAI) of ~6.5 m^2m^{-2}, a stand density of ~1400 trees ha^{-1}, and an average diameter at breast height (DBH) of ~0.16 m (Bäck et al., 2012; Launiainen et al., 2013). The forest floor is majorly covered with a shallow dwarf shrub (a LAI of ~0.5 m^2m^{-2}) and moss layer (a LAI of ~1 m^2m^{-2}) (Kulmala et al., 2008; Launiainen et al., 2013). The planetary boundary layer height at the SMEAR II station has been determined from previous studies using radiosondes (Lauros et al., 2007; Ouwersloot et al., 2012) and balloon soundings (Eerdekens et al., 2009). Roughly, these heights span some 400 m (March) to 1700 m (August) at noontime, and 100 m (March) to <160 m (April) at midnight.

3.2 Instrumentation

Concentration of HOM molecules were measured with two nitrate-ion based CI-APi-TOF mass spectrometers. The CI-APi-TOF measuring at higher altitude was deployed at the top of a 35 m tower located ~20 m horizontally from the ground measurement location. Both instruments were working in rooms with air-conditioning and room temperatures controlled at 25 °C. The inlets of the two instruments were pointed to the southeast direction and fixed at ~36 m and ~1.5 m above ground. The tower measurement is about twice the canopy height, which is still within the roughness sublayer of the forest (Raupach and Thom, 1981). The instrument setup of the two CI-

APi-TOF mass spectrometers were similar. In brief, the CI-APi-TOF was the combination of a chemical ionization (CI) inlet, and an atmospheric pressure interface time-of-flight (APi-TOF) mass spectrometer (Aerodyne Research Inc., USA, and Tofwerk AG, Switzerland). The ambient air was first drawn into the inlet with a sample flow of 7 lpm (liter per minute), and then centered to an ion reaction tube surrounded by sheath flow (filtered air, 35 lpm). Meanwhile, the nitrate ions carried by the sheath gas, which were generated by exposing the nitric acid (HNO_3) to soft x-ray radiation, were guided into the sample gas by an electrical field at ambient pressure (~100 ms reaction time). Neutral molecules (M) in the sample air were ionized by either clustering with charged nitrate/nitric acid ($(HNO_3)_{n=0-2}\cdot NO_3^-$) to form $(M)\cdot NO_3^-$ cluster ions, or losing a proton to the charging ions to form deprotonated ions (e.g., $H_2SO_4+NO_3^- \rightarrow HSO_4^- + HNO_3$). The ions then entered the APi part, which was a three-stage vacuum chamber, through a pinhole. In the APi, two quadrupoles and stack of ion lenses guide the ions into the TOF mass spectrometer, where ions were separated based on their mass-to-charge (*m/z*) ratios. A more detailed description of this instrument has been given by Junninen et al. (2010) and Jokinen et al. (2012). Mass spectra obtained from the instrument were analyzed using the 'tofTools' program described in Junninen et al. (2010). Determination of the concentration of a measured molecule M was based on the following equation:

$$[M]=\frac{\sum M}{\sum reagent\ ion\ count\ rates}\times C \quad (1)$$

where the sum of ion count rates was an inclusion of all detected ions relating to compound M, whether deprotonated or in clusters with reagent ions, and the sum of reagent ion count rates is the total signal of the charged nitric acid ions. C was the calibration coefficient, which was assigned the same value for all detected compounds. This assignment is only valid for compounds that cluster with the reagent ions at the collision limit, such as H_2SO_4 (Viggiano et al., 1997) and have equal collision rates. The collision rates of nitrate ions with H_2SO_4 and with HOMs are expected to be very close (Ehn et al., 2014). Here, a calibration coefficient of 1×10^{10} molec cm^{-3}, estimated

166 from previous calibrations with similar settings using sulfuric acid and theoretical
167 constraints (Ehn et al., 2014), with an uncertainty of at least -50%/+100%, was used in
168 calculating the HOM concentrations for both instruments. Ultimately, the absolute
169 HOM concentrations in this work are of secondary importance, as we focus on the
170 relative comparison of HOM concentrations measured at different heights. However,
171 the comparability of the two CI-APi-TOF instruments is of great importance, and
172 results cannot be allowed to vary e.g. as a result of inevitable differences in the mass-
173 dependent transmission efficiency (TE). For a detailed discussion on factors affecting
174 the TE of a CI-APi-TOF, we refer to Heinritzi et al. (2016). To this end, instead of
175 directly evaluating the TE of each instrument, a "relative" TE of the two CI-APi-TOFs
176 was used for data correction: we selected a time period at noon-time on September 9
177 with well-mixed boundary layer condition, identified with the clear and sunny weather
178 and homogeneous vertical distribution of monoterpene and other trace gases., and
179 assumed the HOM concentrations at the two heights to be the same. Thus, the relative
180 TE was obtained from the concentration ratio between the two CI-APi-TOFs at each
181 *m/z* (Figure 1). A fitted relative TE curve ($R^2 = 0.97$), which represents how the TE of
182 the tower CI-APi-TOF was changed at each m/z over the TE of the ground one, was
183 obtained using power law regression. Weaker correlation was obtained in the 200-250
184 and 500-600 Th mass ranges, but in the mass range where most of the HOMs were
185 located (290-500 Th) there is very little scatter around the fitted curve, clearly
186 suggesting that observed differences in the two instruments responses were mainly due
187 to differences in TE. To test our assumption of negligible vertical gradients of HOMs
188 during daytime, we analyzed the behavior of sulfuric acid. We found that the
189 uncertainty related to this assumption corresponds to a value of 26% (see Figure S1).
190 An upper limit of uncertainty relating to our TE correction (Figure 1) was also estimated,
191 yielding a value of 10%, giving a total uncertainty from these two sources of 28%. This
192 value is much smaller than the observed deviation of HOM concentrations during
193 inversion nights (e.g. Figure 5). Additionally, an inter-comparison between the two

instruments with a permeation tube containing trinitrotriazinane ($C_3H_6N_6O_6$) was conducted in the field right after the campaign. The results showed good agreements with the relative TE, lending confidence to the method used here. Finally, it should be noted that the difference in TE between the two instruments was larger than one would normally expect, since the tower CI-APi-TOF had been tuned for higher sensitivity at the largest masses (at the expense of transmission at the lower masses).

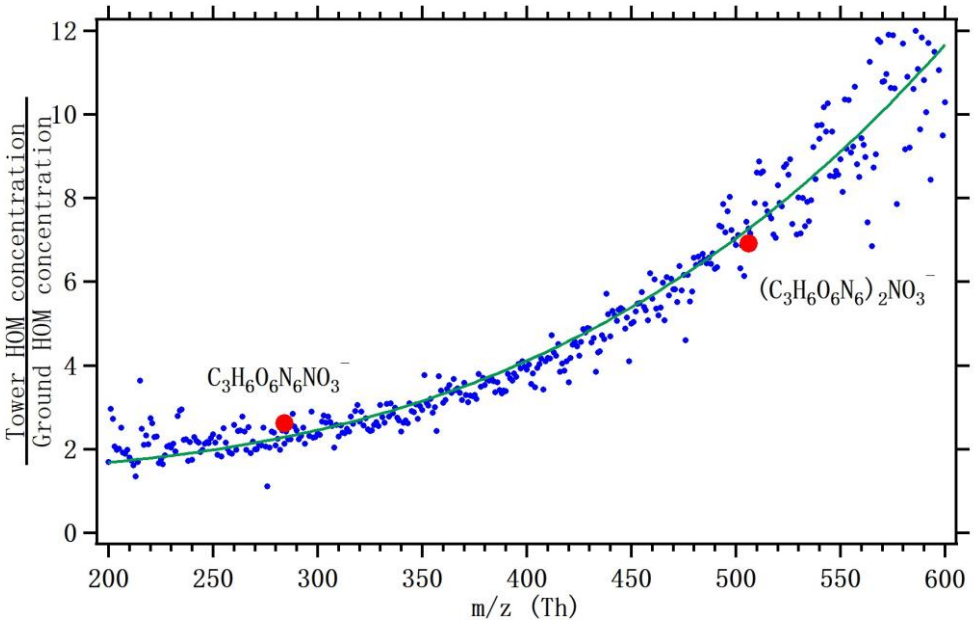

Figure 1 The relative TE curve between the two CI-APi-TOF mass spectrometers. Inter-comparison results using a permeation tube containing trinitrotriazinane ($C_3H_6N_6O_6$) are shown in red circles.

In comparison to the direct determination of TE (Heinritzi et al., 2016), this method increases the uncertainty in the quantification of HOM concentrations. However, as mentioned, a more accurate knowledge of the exact HOM concentrations would not influence the main findings of this study.

The MT, trace gases, and meteorological parameters were continuously monitored at the different heights (4.2 m, 8.4 m, 16.8 m, 33.6 m, 50.4 m, 67.2 m, 101m, and 125 m) on a 126 m mast ~100 m away from the location of the CI-APi-TOFs. The data at 4.2

m and 33.6 m were used in this study to represent the concentrations at near ground and tower level, respectively. Ambient MT concentration was measured every third hour using a proton transfer reaction mass spectrometer with a lower detection limit of 1 pptv (PTR-MS, Ionicon Analytik GmbH; Taipale et al., 2008). The O_3 concentration was measured with an UV light absorption analyzer that had a lower detection limit of 1 ppbv (TEI model 49C, Thermo Fisher Scientific, USA). The NO_x measurement was conducted using a chemiluminescence analyzer (TEI model 42C TL, Thermo Fisher Scientific, USA). The lower detection limit of the NO_x analyzer is 100 pptv. The CO_2 measurement was performed using an infrared detection system (LI-840, LiCor Biosciences, Lincoln, NE, USA). The aerosol number concentration size distributions were obtained with a twin differential mobility particle sizer (twin-DMPS) for the size range from 3-1000 nm (Aalto et al., 2001) at 8 m height above ground, and was used to calculate condensation sink (CS) based on the method from Kulmala et al. (2001). Air temperature was measured with PT-100 resistance thermometers. Air relative humidity (RH) was measured with RH sensors (Rotronic Hygromet model MP102H with Hygroclip HC2-S3, Rotronic AG, Switzerland). Global radiation (solar radiation in wavelength range of 0.3-4.8 μm) was obtained with a Pyranometer (Reemann TP3, Astrodata, Estonia) above the canopy top at 18 m. All the data presented are at 10 min averaging intervals, except for the MT (in 1-hour averaging interval). A schematic figure showing locations of all the measured parameters is provided in Figure S2.

4 Results and discussion

4.1 Data overview

The Influence of Biosphere-Atmosphere Interactions on the Reactive Nitrogen budget (IBAIRN) campaign was conducted from September 1 to 25, 2016. After data quality checks, only the measurements collected after September 5 were used. Figure 2 shows the overall time series of the meteorological parameters measured at ground and tower

levels, including the temperature, RH, global radiation, concentrations of trace gases, MT, and total HOMs. The weather was generally sunny and clear during the campaign except for a few cloudy (September 10, 15, and 22-23) and drizzling (September 24 and 25) days. The mean air temperature and RH observed at ground level were 10.8 ± 3.3 ℃ and 87 ± 13 % (1σ standard deviation), and at the tower level were 10.5 ± 3.0 ℃ and 88 ± 14 %, respectively. The O_3 concentrations measured at ground and tower levels were 21 ± 8 ppbv and 25 ± 6 ppbv, respectively. The air temperature, RH and O_3 measured at the two heights were close to each other during daytime. The NO_x concentrations were quite low throughout the campaign, the mean NO_x concentrations were mostly around the reported detection limit at 0.4 ± 0.4 ppbv (ground) and 0.4 ± 0.5 ppbv (tower), yet showed an overall good agreement between the measurements at the different heights. The MT concentrations at ground level (0.38 ± 0.34 ppbv on average) were generally higher than that above the canopy level (0.20 ± 0.16 ppbv).

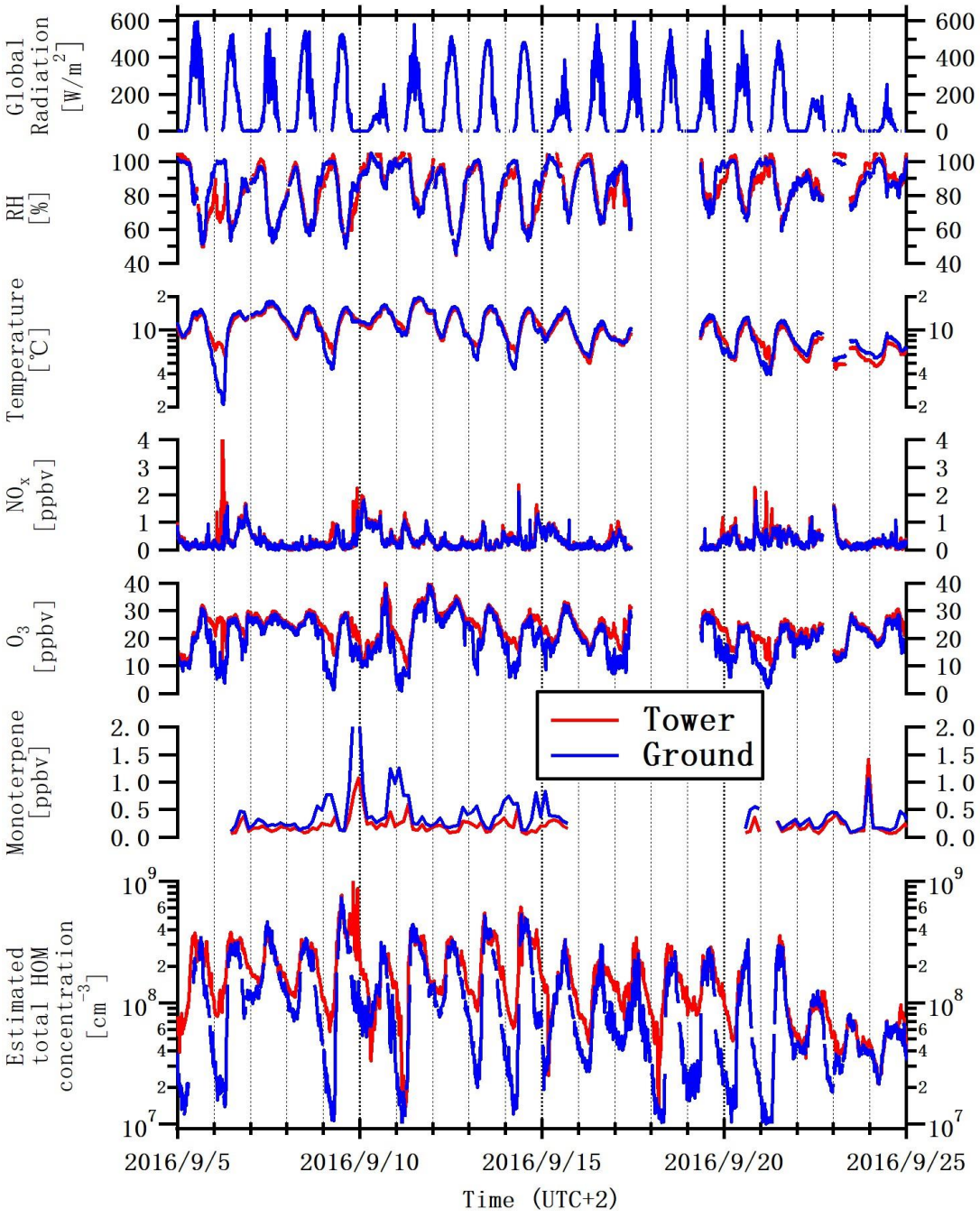

Figure 2 The overall time series of the measured trace gases, meteorological parameters and estimated total HOM concentrations at the ground (blue) and tower (red) levels.

The estimated total HOM concentration is representative for the overall concentration level of HOMs, and is defined as the sum of the detected signals between ions from *m/z* 200 to 600 after removing the identified background peaks. The gaps in the ground estimated total HOM data were due to automatic zero-check. During the campaign, a

significant difference was found in the estimated total HOM concentrations below and above the canopy (mean and median concentrations of $1.1 \pm 1.7 \times 10^8$ cm^{-3} and 7.6×10^7 cm^{-3} at ground level, $1.7 \pm 1.3 \times 10^8$ cm^{-3} and 1.3×10^8 cm^{-3} at tower level). The causes of these differences (~ 55% in mean and ~71% in median) frame the upcoming discussion.

4.2 Inter-comparison of estimated total HOM concentrations

The estimated total HOM concentrations at the two heights were not different during the day (mean ± 1σ standard deviation and median concentrations of $4.1 \pm 2.3 \times 10^8$ cm^{-3} and 3.6×10^8 cm^{-3} at ground level, $4.3 \pm 2.6 \times 10^8$ cm^{-3} and 4.0×10^8 cm^{-3} at tower level), which validates the use of only one day of data for scaling the TE of the ground CI-APi-TOF to match the HOM signals. The good daytime agreement throughout the campaign period also verifies that the response of each instrument stayed stable. Contrary to the daytime results, the estimated total HOM concentration at ground level usually diverged from the tower measurement in the nocturnal boundary layer. The concentration below the canopy became even lower when temperature inversions were observed, accompanied by a decreasing ground-level O_3 and increasing MT concentrations. Figure 3 shows the correlation between the estimated total HOM concentrations observed at two heights. Herein, good agreement could be found for the group of points representing the concentrations around noontime (R^2 = 0.89). The points indicating the nighttime estimated total HOM concentrations were scattered (R^2 = 0.28), and the ground concentrations were found to be much lower than the tower ones.

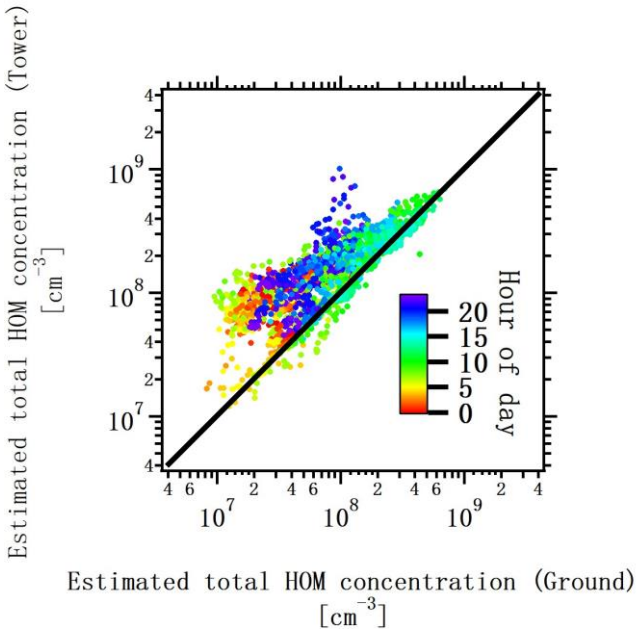

Figure 3 Correlation between ground (x-axis) and tower (y-axis) measurements of the estimated total HOM concentrations. The black line denotes 1:1 ratio. Color code indicates the sampling time of HOMs.

Figure 4 shows the mean mass spectra (in unit mass resolution, UMR, for *m/z* 200 – 600) obtained from the ground and tower. It is worth mentioning that there might be some signals not attributable to HOMs in the plotted spectra, but only in little proportion. Only selected periods (09:00-15:00 for daytime and 21:00-03:00 for nighttime, local winter time (UTC +2)) are included in the averaging period to eliminate the effect of sunrise and sunset periods. During daytime, a good agreement ($R^2 = 0.87$) was obtained from the mass-by-mass comparison using the UMR concentrations extracted from daytime mean spectra, suggesting a uniform composition distribution in the daytime boundary layer condition. During nighttime, the mean concentrations of all HOM molecules in the ground mean spectra were much lower than the tower spectra. The HOM concentrations shown in the ground and tower mean spectra were also less correlated. Therefore, a logical outcome is that the conditions below and above the canopy are experiencing different turbulent mixing strength and/or source-sink regimes

304 during night.

305

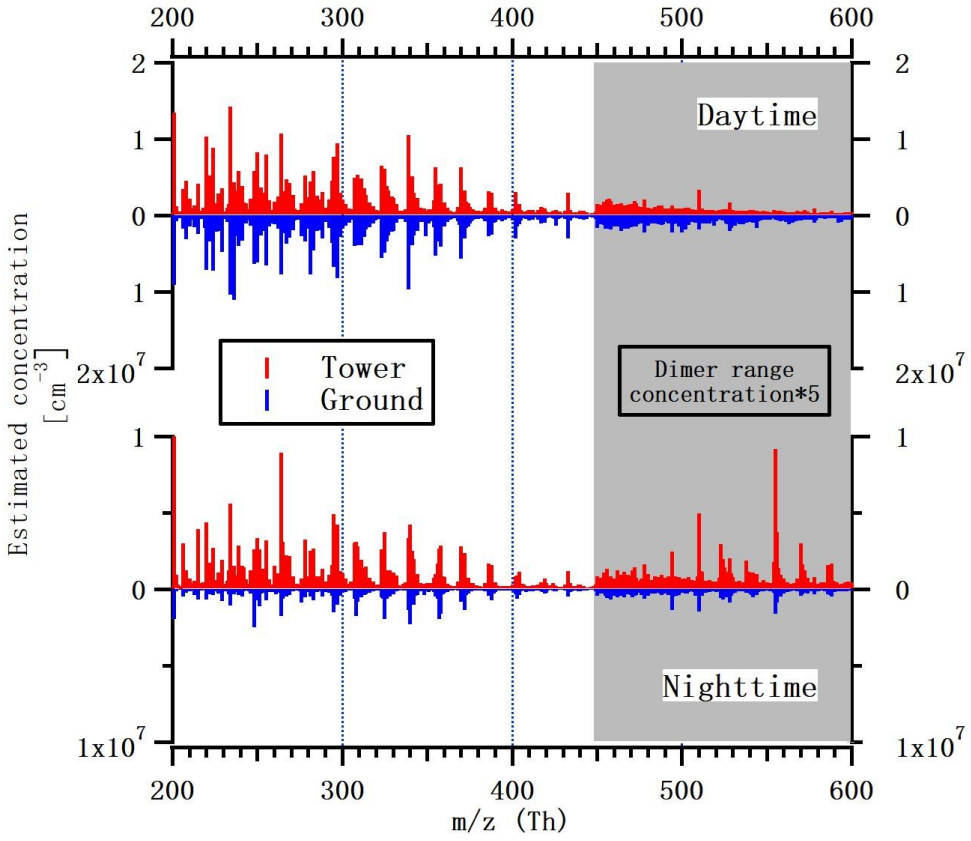

306

307 Figure 4 Mean mass spectra with the averaging periods of daytime (09:00-15:00) and nighttime (21:00-

308 03:00) at ground and tower levels.

309 **4.3 Influence of nocturnal boundary layer dynamics and micrometeorological**

310 **processes**

311 The nighttime HOMs at ground level are likely influenced by transport processes below

312 the canopy, since the estimated total HOM concentrations were found much lower in

313 the nights when temperature inversions were observed. To further investigate the

314 potential impact of such micrometeorological phenomena on ground HOMs, for the

315 nights during the campaign without precipitation or instrument failure, were selected

316 (12 nights in total) and categorized into 2 types based on the occurrence of temperature

317 inversions: 1) the “non-inversion night” type included 6 nights when no temperature

318 inversion was recorded; 2) the “inversion night” type category consisted of 6 nights that

had encountered temperature inversions, and the ground temperatures were generally ~1 ℃ lower than tower temperatures during these nights.

4.3.1 Statistics of the "non-inversion night" and "inversion night" types

Table 1 shows the overall statistics including the mean and median values of the temperatures, O_3, NO_x, MT and estimated total HOM concentrations for the "non-inversion night" and "inversion night" types. In the non-inversion nights, the air below and above the canopy was relatively well-mixed. The mean and median concentrations of the ground O_3 (21 ± 8 ppbv and 22 ppbv) were close to the tower values (25 ± 6 ppbv and 24 ppbv). The slight difference might be attributed to the higher VOC emissions (Rantala et al., 2014) and larger sink near ground level. In contrast, during the inversion nights, the mean estimated total HOM concentration and O_3 at ground level were generally much lower, only ~33% and ~69% of the tower concentrations, respectively. Instead, the mean and median ground MT concentration (0.70 ± 0.28 ppbv and 0.70 ppbv) were ~3 times higher than the tower ones (0.24 ± 0.04 ppbv and 0.23 ppbv), respectively. The measured NO_x levels were similar in both categories and heights, though the ambient concentrations were close to the detection limit and therefore small differences might not be observable.

4.3.2 Case study

Two individual nights representing the "non-inversion night" and "inversion night" types were selected and further compared. Figure 5a shows the time series of the meteorological parameters, trace gases and HOMs measured at ground and tower levels of one selected night of "non-inversion night" type (September 11-12, from 21:00 to 03:00). A number of measures can be used to assess the local atmospheric stability conditions at a given layer. These measures are commonly based on either the Obukhov

length and its associated atmospheric stability parameter or a Richardson number (flux-based, gradient-based, or bulk). Because of its simplicity and the availability of high resolution mean air temperature profiles, the bulk Richardson number (Ri) was used here (Mahrt et al., 2001; Mammarella et al., 2007; Vickers et al., 2012; Alekseychik et al., 2013). It is calculated using:

$$Ri = \frac{g\Delta\overline{\theta}\Delta z}{\overline{\theta}(\overline{u})^2} \quad (2)$$

where g is the gravitational acceleration, $\Delta\overline{\theta}$ and Δz are the mean potential temperature (10 min averaging interval, same as measurement data) and height difference between the ground and tower levels, respectively, $\overline{\theta}$ and $\overline{u}$ are the mean potential temperature and mean wind velocity at tower level, respectively. During the selected "non-inversion" night, Ri was generally positive but close to 0 (shown in Figure 5a), indicating a weakly stable and relatively well-mixed (i.e. $\Delta\overline{\theta} \to 0$) condition (Mahrt, 1998; Mammarella et al., 2007). This was also confirmed using the well correlated ground and tower MT and trace gases concentrations.

Table 1 Summary of the "Non-inversion night" and "Inversion night" types.

Type		**Non-inversion night**					**Inversion night**				
Date		September 6, 7, 9, 11, 15, 16, 21*					September 5, 8, 10, 12, 13, 14, 19**				
Parameters		Temperature [°C]	O_3 [ppbv]	NO_x [ppbv]	MT [ppbv]	Estimated total HOM [10^8 cm^{-3}]	Temperature [°C]	O_3 [ppbv]	NO_x [ppbv]	MT [ppbv]	Estimated total HOM [10^8 cm^{-3}]
Tower	Mean ± 1σ standard deviation	10.2 ± 2.6	25 ± 6	0.5 ± 0.5	0.31 ± 0.31	2.9 ± 1.9	9.5 ± 1.7	24 ± 2	0.4 ± 0.3	0.24 ± 0.04	2.4 ± 0.8
	Median	10.9	24	0.4	0.17	2.8	9.2	23	0.3	0.23	2.3
Ground	Mean ± 1σ standard deviation	10.6 ± 2.7	21 ± 8	0.4 ± 0.4	0.52 ± 0.74	1.6 ± 0.6	8.3 ± 2.2	16 ± 6	0.3 ± 0.2	0.70 ± 0.28	0.8 ± 0.4
	Median	11.5	22	0.3	0.22	1.7	8.5	17	0.3	0.70	0.7

*MT data not available on September 5 and 19.

**MT data not available on September 15 and 16

Selected HOM molecules representing the major HOM types (and formation pathways) were summed up and categorized into 4 groups, as shown in Table 2. Each pathway might be influenced differently by boundary layer dynamics and micrometeorological processes. In this study, OH-initiated HOMs were assumed negligible due to the very low OH level in the nocturnal boundary layer.

Table 2 Compositions of selected HOM molecules and their main oxidants (Yan et al., 2016).

	Molecule compositions	**Main oxidants**	**Main terminators**
$CHO_{monomer}$	$C_{10}H_{14}O_7$, $C_{10}H_{14}O_9$	O_3	Self-terminate or RO_2
$CHON_{monomer}$	$C_{10}H_{15}O_9N$, $C_{10}H_{15}O_{11}N$	O_3 or NO_3	NO or Self-terminate/RO_2
CHO_{dimer}	$C_{19}H_{28}O_{11}$, $C_{20}H_{30}O_{14}$	O_3	RO_2
$CHON_{dimer}$	$C_{20}H_{32}O_{12}N_2$, $C_{20}H_{31}O_{13}N$	NO_3	RO_2

All the HOM groups in Figure 5a show stable patterns, and good agreement is observed between the ground and tower measurements in the first half of the night. Variations were observed when air mass change occurred at around 01:00, as indicated by the drop of NO_x concentration and horizontal wind shift (not shown here). A rapid decrease was found in CS, which represents the rate of condensation of low-volatile vapors onto the existing aerosol particles (Dada et al., 2017), implying that the aerosol population also altered. However, the HOM groups were still well correlated with each other, suggesting the unchanged well-mixed condition in the non-inversion night.

Figure 5b shows the time series of the trace gases, MT, and HOM groups of both ground and tower measurements during an "inversion night" case (September 8-9, from 21:00 to 03:00). *Ri* was generally higher during this night, and increased from ~0.03 (indicating weakly stable condition, Mammarella et al., 2007), at around midnight, to a maximum of ~1.13 (indicating very stable condition) in the remaining night period. Roughly, *Ri* values in excess of unity indicate that stably stratified conditions

appreciably diminish the inverse turbulent Prandtl number (*Pr*) and the efficiency of turbulence to mix heat when compared to momentum (Katul et al., 2014). The parameters measured at tower level were not significantly affected by strong *Ri* fluctuations throughout the night, in contrast, significant variations were observed at ground level.

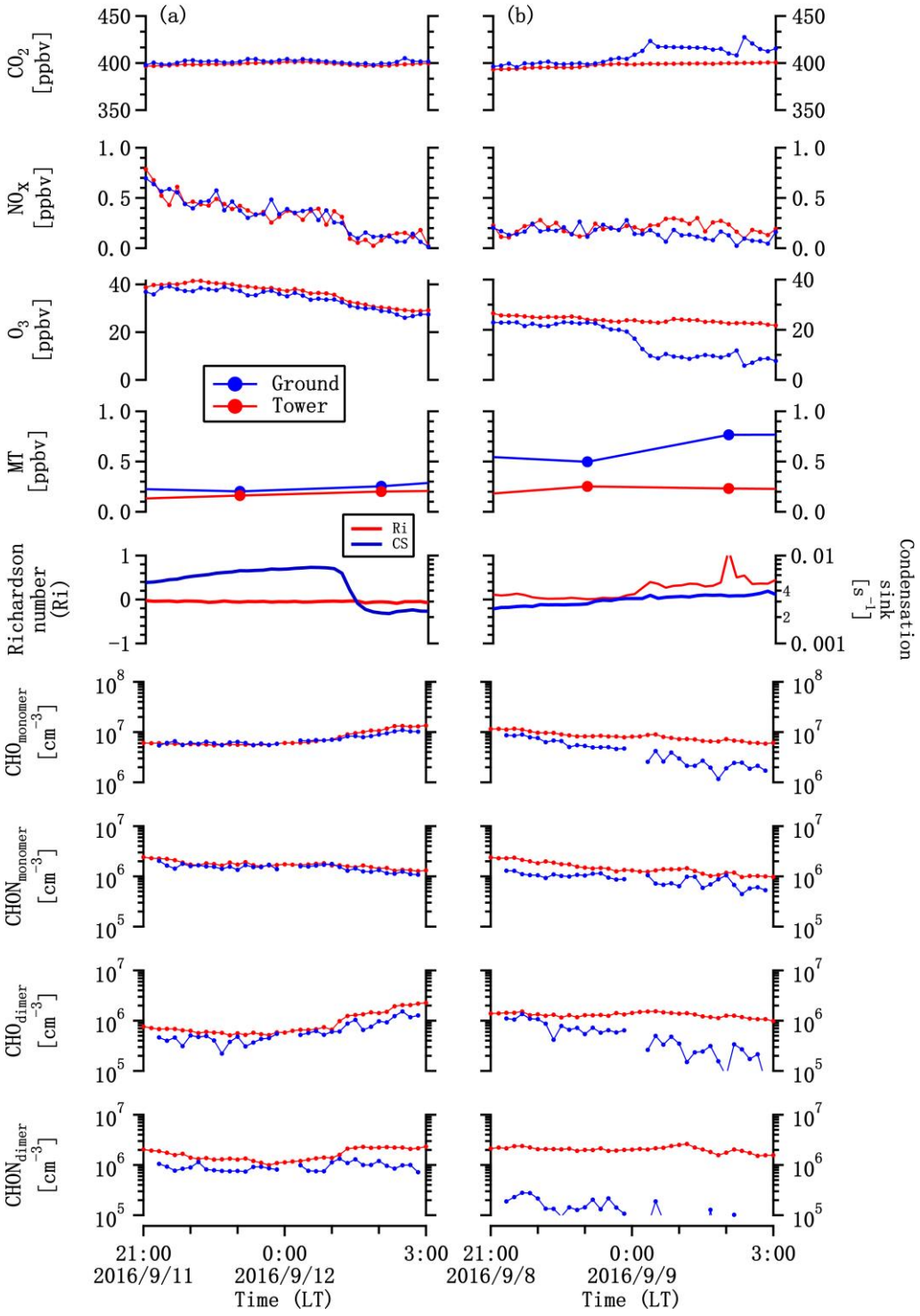

Figure 5 (a) Time series of ground and tower concentrations of CO_2, NO_x, O_3, MT, and selected HOM groups in the selected "non-inversion night" (September 11), and (b) "inversion night" (September 8). *Ri* is calculated with the meteorology data of ground and tower levels. CS is determined based on the aerosol data measured at 8 m above ground level.

The ground O_3 concentration experienced a rapid decrease at midnight. In about an hour

(from 23:30-00:30), ground O_3 concentration dropped by more than half (from 20 ppbv to 9 ppbv), and CO_2 concentration increased as well (from 404 ppbv to 423 ppbv). To the contrary, the MT concentration at ground level was almost doubled (from 0.49 ppbv to 0.80 ppbv) during the same period. Theoretically, the enhancement of HOM precursor and decrease of oxidant would compensate each other if the sink remained the same, and the ground HOM concentrations should also keep constant. However, all the HOM groups showed significant decrease after midnight, despite the CS (generally the main sink for HOM in the atmosphere) staying practically constant. In particular, the concentration of the $CHO_{monomer}$ group dropped ~80%, from 8.6×10^6 cm^{-3} to 1.7×10^6 cm^{-3}, and the concentration of the CHO_{dimer} group decreased from 1.5×10^6 cm^{-3} to ~1.0×10^5 cm^{-3}. The concentrations of the $CHON_{monomer}$ and $CHON_{dimer}$ groups also experienced large declines (~34% and ~50%, respectively), in the latter half of the night. At 03:00, the $CHON_{dimer}$ concentration was already below the detection limit (1×10^4 cm^{-3}). Therefore, the much lower ground HOM concentrations might not be totally explained by the change of HOM production, but also due to some other processes such as additional losses.

A previous study by Alekseychik et al. (2013) at SMEAR II station showed that nocturnal decoupled air layers were frequently (with a fraction of 18.6% based on a long-term dataset) observed under high Ri conditions in the boreal forest. The decoupled layer could strongly influence the ground O_3, MT, and CO_2 concentrations (Rannik et al., 2009, 2012; Alekseychik et al., 2013; Chen et al., 2018), and could also explain the occurrence of the strong temperature inversion during the inversion nights. To explore the possible mechanism resulting in significantly different O_3, MT and HOM concentrations below the canopy, the mean continuity equation for high Reynolds number flows within the canopy is formulated as (e.g. Katul et al. 2006):

$$\frac{\partial \bar{C}}{\partial t} + \bar{U}\frac{\partial \bar{C}}{\partial x} + \bar{W}\frac{\partial \bar{C}}{\partial z} = -S - \frac{\partial \overline{w'c'}}{\partial z} - \frac{\partial \overline{u'c'}}{\partial x} \quad (3)$$

$$N_1 + N_2 + N_3 = N_4 + N_5 + N_6 \quad (4)$$

where t is time, x and z are the longitudinal and vertical directions, respectively, C

is the scalar concentration, U and W are the longitudinal and vertical velocity components, $\overline{w'c'}$ and $\overline{u'c'}$ are the turbulent scalar fluxes in the vertical and horizontal, respectively, and S represents the net sources or sinks (physical, chemical, and biological) of C, and overline represents time averaging over turbulent scales. The 6 terms in this equation represent the following (left to right): local rate of change($= N_1$), horizontal advection by the mean velocity $(= N_2)$, vertical advection by the mean velocity $(= N_3)$, net sources or sinks $(= N_4)$, net vertical transport by the vertical turbulent flux gradient $(= N_5)$, net horizontal transport by the horizontal turbulent flux gradient $(= N_6)$. Generally, $|N_6| \ll |N_5|$, and is hereafter ignored in the discussion.

During the non-inversion night, the ground O_3 could be replenished either by vertical turbulent transport (N_5), mean vertical advection from upper boundary layer (N_3), or horizontal advection below the canopy (N_2) (as shown in Figure 6). However, for highly stratified flows, N_5 becomes small, as the efficiency of turbulence to transport O_3 to layers near the ground becomes weak (Katul et al., 2014). Vertical and horizontal advection were also small within such a stable layer, and the reduced mean velocity would result in smaller contributions from N_2 and N_3. Note that these advective terms tend to be opposite in sign by the virtue of the mean fluid continuity equation (Katul et al., 2006). Instead, the sink of O_3 (N_4) was stronger because of the increasing loss due to a higher surface area-to-volume density (S/V) in this shallow decoupled layer. Under this circumstance, the ground O_3 concentration dramatically decreased when the air layer was forming, and eventually reached a much lower concentration. The decoupled layer also affected MT and CO_2 below the canopy in the inversion night, but resulted in concentration increases as opposed to O_3. The weakened vertical turbulence (N_5) tended to retain the emissions from ground and understory vegetation within the layer, though N_4 also increased. In general, the increased CO_2 (primary source from the ground) and MT (primary source from the canopy) at ground level are good indicators for the extent of the mixing in the shallow decoupled layer. At the same time, the strong decrease of O_3 shows how the sinks in this layer are no longer balanced by a large flux

of O_3 from upper layers. However, the stabilization of ground-level O_3 concentrations at non-zero values after the initial fast decrease suggests that a small amount of inflow, either via N_3 or N_5, is still taking place.

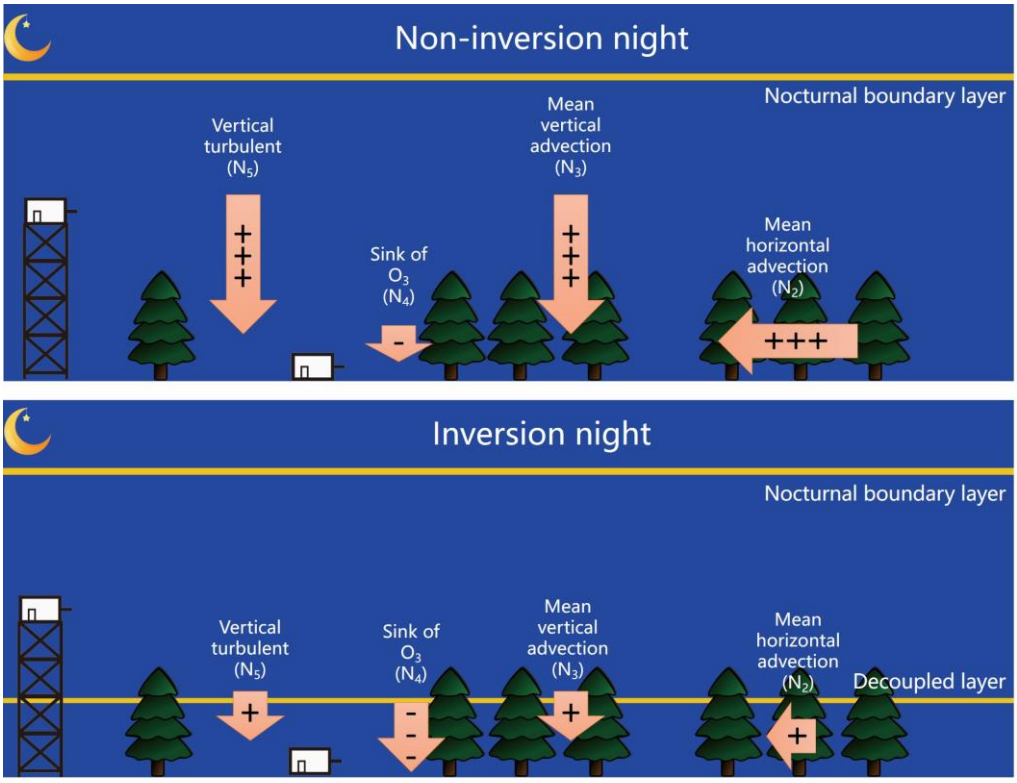

Figure 6 Schematic figure showing how vertical mixing, vertical advection, and horizontal advection influence ground O_3 concentrations differently in non-inversion night and inversion night at SMEAR II station.

Therefore, the differences between the ground and tower measurements were due to the joint effects of: (i) decoupling between the stably stratified near-ground layer and the canopy top, and the consequent formation of a shallow layer, (ii) weakening of advective and turbulent flux transport terms thereby inhibiting mass exchange between the ground decoupled layer and the remaining nocturnal boundary layer, and (iii) increased surface area to volume within the decoupled layer thereby enhancing N_4.

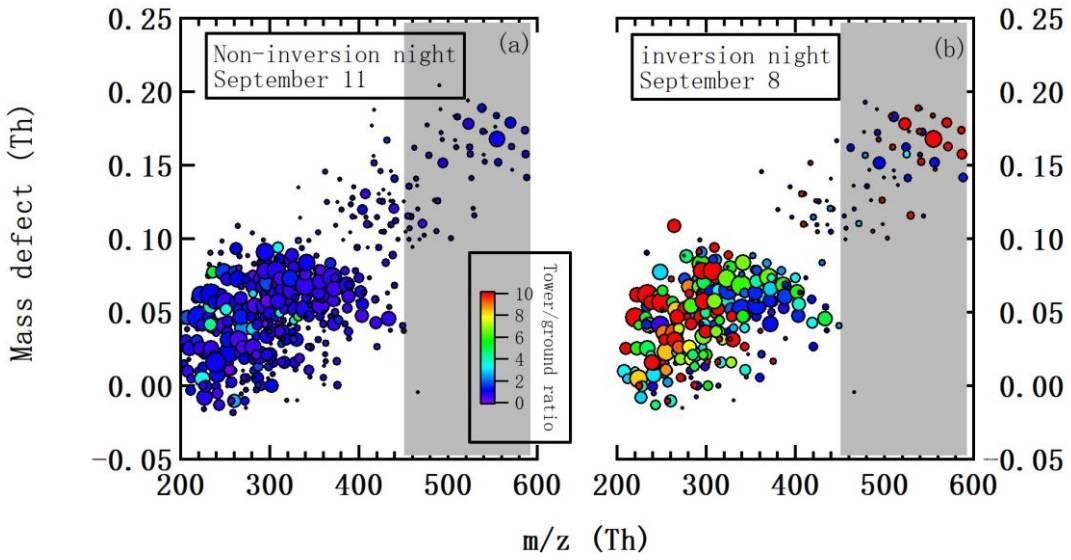

Figure 7 Mass defect (MD) plots of the selected (a) "non-inversion night" case (September 11), and (b) "inversion night" case (September 8). Color code indicates the ratios between tower/ground HOM concentrations. Grey shade area denotes the dimer range (*m/z* 450-600).

Examination of the selected HOM molecules was useful and efficient to assess the changes in HOMs, however, such an analysis might only indicate the major formation pathways. Hence, it was also worthwhile to have a holistic view of the entire mass spectra and all the detected HOMs. The mass defect (MD) plot (Figure 7) separates all identified compounds according to their exact masses on the x-axis and the deviation from the integer mass on the y-axis. Each circle represents a compound, with the areas scaled by concentrations, and colored by the ratios between tower and ground concentrations. Figure 7a and 7b are MD plots showing the mean spectra of the selected non-inversion night (September 11) and inversion night (September 8). Without the formation of a decoupled layer, nearly the same concentration distributions of HOMs were observed. In contrast, during the inversion night (September 8, Figure7b), large differences could be found between the two measurement heights. Moreover, a significant fraction of the ground HOMs disappeared on the inversion night, and the concentrations of the remaining HOMs were also lower, confirming the aforementioned results obtained with the selected HOM groups.

4.4 Study limitations

Several limitations still exist in this study. From the measurement side, one major concern was the comparability between our two CI-APi-TOF mass spectrometers. In the worst case, our conclusion might be biased if instrument responses changed due to some parameter that correlated with the observed inversions. The main parameters in this case would be ambient temperature and RH. As both instruments were located in temperature-controlled containers and the sample flow was mixed 1:2 with dry sheath air in the CI-APi-TOF drift tube, neither of these were expected to yield such large changes. However, for confirmation, we compared the detailed spectral evolution during days and nights of the study. Figure 8 shows an example of hourly changes of the ratios between tower and ground HOMs, over a 24h period without nighttime temperature inversion (September 11). During this period, ambient temperatures changed from 19.1 °C (12:00 LT) to 8.8 °C (07:00 LT) at ground level, and from 17.9 °C to 8.1 °C at tower level. Ambient RHs also increased from 72 % to 96 % at ground level, and from 74 % to 98 % at tower level. While some scatter is visible in the 200-300 Th range during some parts of the night, good agreement was observed between the two instruments throughout the night, despite large variability in temperatures and RHs.

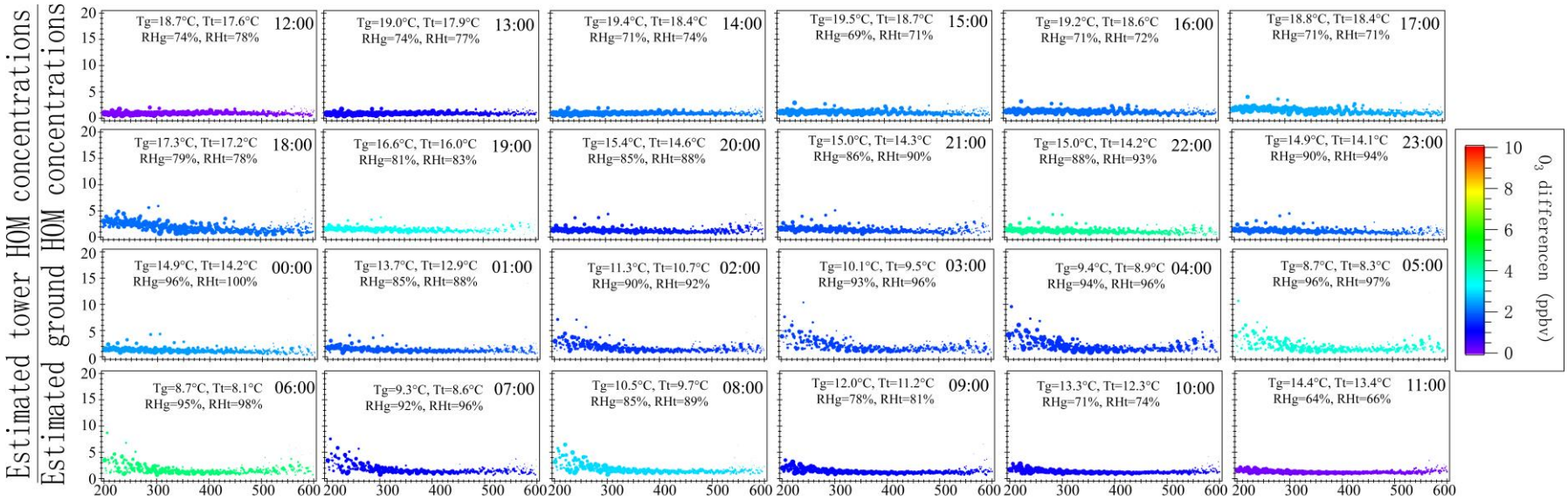

Figure 8 Hourly changes of the ratios between estimated tower and ground HOM concentrations from September 11, 12:00 to September 12, 11:00 (non-inversion night). Markers are sized by ground HOM concentrations and colored by O_3 difference between tower and ground $(O_{3_{\text{tower}}} - O_{3_{\text{ground}}})$. Hourly ambient temperatures at ground (Tg) and tower (Tt) levels, and RH at ground (RHg) and tower (RHt) levels are shown in each subplot.

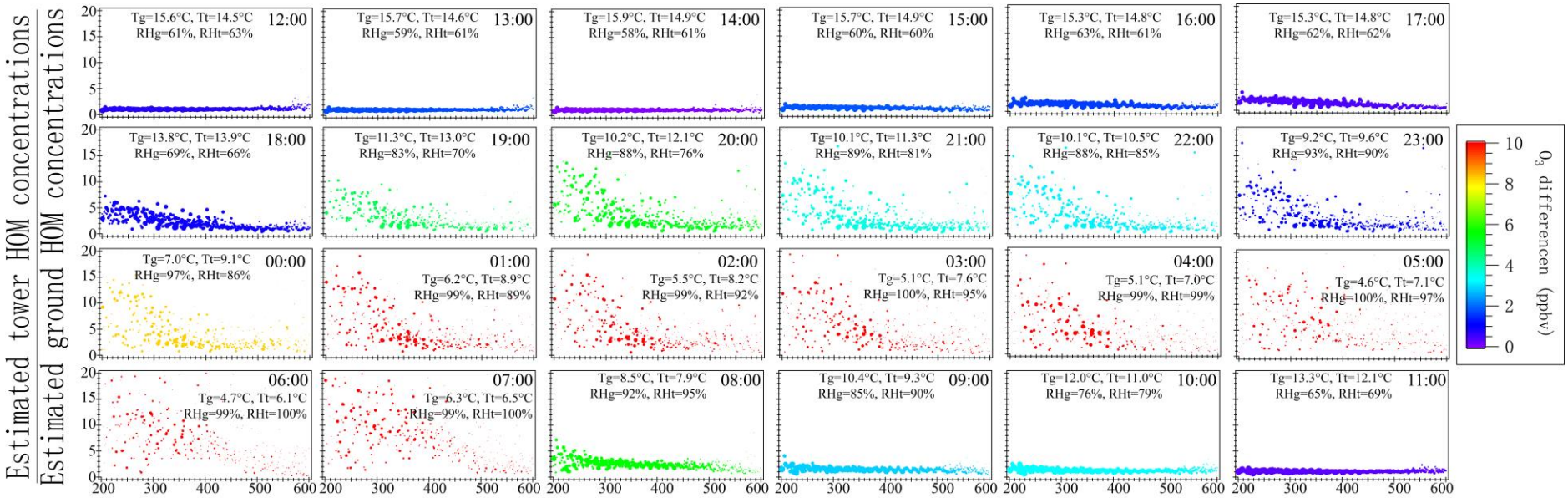

Figure 9 Hourly changes of the ratios between estimated tower and ground HOM concentrations from September 8, 12:00 to September 9, 11:00 (inversion night). Markers are sized by ground HOM concentrations and colored by O_3 difference between tower and ground ($O_{3_{\text{tower}}} - O_{3_{\text{ground}}}$). Hourly ambient temperatures at ground (Tg) and tower (Tt) levels, and RH at ground (RHg) and tower (RHt) levels are shown in each subplot.

In contrast, during a 24h period with nighttime temperature inversion (September 8, shown in Figure 9), the ratios agreed well only during daytime (from 12:00 to 17:00, and 09:00-11:00 on the next day). Between these periods, temperature and RH were most of the time in the same range as on September 11 (when no strong deviations were observed), but now the HOM behavior changed dramatically between the two heights. The ratios increased from ~1 (during daytime) up to ~20 at 07:00 for some of the measured molecules.

Figures 8 and 9 clearly imply that the large differences between ground and tower HOM concentrations were driven by temperature inversions and consequent changes in the composition of the air in the two detached layers. Large changes in HOMs were observed only when the ground temperature was lower than the tower temperature and when the ozone concentration at ground level was several ppb lower. Absolute temperatures or RHs at the two heights were not able to explain the changes. As a concrete example, good agreement was observed at 07:00, September 12, while ambient temperatures were low (ground and tower temperatures were 9.3 ℃ and 8.6 ℃, respectively) and RHs were high (ground and tower RHs were 92 % and 96 %, respectively), but large deviations were found at 20:00, September 8, when higher temperatures (ground and tower temperatures were 10.2 ℃ and 12.1 ℃, respectively) and lower RHs (ground and tower RHs were 88 % and 76 %, respectively) were observed. In other words, neither low temperatures nor high RHs caused large changes to our instruments. Instead, the large discrepancies between the two CI-APi-TOFs were only observed when other key parameters (like ozone) were found to deviate considerably between the two heights.

From micrometeorology side, the contribution from the potential micrometeorological processes in the layer between 1.5 m and 4.2 m (between the sampling heights of the ground HOMs and other parameters) could not be estimated with the current experiment

346 design (i.e., only two measurement heights). Similarly, the influence from horizontal
347 advection could not be entirely ruled out as a contributor to the reduced ground-level
348 HOM concentrations (and other significantly changed species), because of the possible
349 horizontal inhomogeneity of HOM precursors and oxidants below the canopy. However,
350 our conclusion was confirmed by the incompatibility between the increasing ground
351 MT and CO_2 concentrations and the advection hypothesis (i.e., all species would show
352 similar tendencies if advection played a major role), indicating the influence of
353 horizontal and vertical advection is probably minor when compared to the increasing
354 sink. However, more direct evidence is still needed for further validation, which
355 highlights the need for joint vertical-planar HOM studies, measuring both vertical and
356 horizontal distribution of HOM concentrations.
357

358 **5 Conclusion**

359 Highly oxygenated molecules (HOMs) were measured above the canopy and at ground
360 level (below the canopy) in a boreal forest environment during the IBAIRN campaign
361 that took place in September 2016. Boundary layer dynamics and micrometeorology
362 were found to be important factors that influence the abundance and trends of HOMs
363 at ground level, by perturbing both their sources and sinks. In the well-mixed boundary
364 layer (e.g. during daytime or nights without strong inversion), HOM concentrations and
365 other measured species were overall similar between the ground and tower
366 measurements. In contrast, much lower ground level HOM concentrations were
367 observed when nighttime temperature inversion and formation of a decoupled layer
368 occurred below the canopy. On one hand, the production of the ground-level HOMs
369 could be affected by the decreasing O_3 concentrations and the increasing MT
370 concentration in the shallow layer. On the other hand, the surface area to volume ratio
371 dramatically increased in the shallow layer compared to the nocturnal boundary layer.
372 The possibility of losses on surfaces for ground-level HOMs became much larger than

usual during inversion nights. The enhanced interaction of air in the decoupled layer with the forest floor was supported by increased concentrations of CO_2, emitted mainly from the ground, in this layer.

We have presented the first detailed measurements of HOMs below and above the canopy across a wide range of atmospheric stability conditions. The results highlight the significance of near-ground boundary layer dynamics and micrometeorological processes to the ambient HOMs, showing that ground-based HOM measurement at this site might not be representative for the entire nocturnal boundary layer. Conventionally, field measurements of HOMs and other parameters are mostly performed close to the ground, and the possible effect of boundary layer dynamics and micrometeorological processes to the HOM concentrations have rarely been considered. Aerosol particle growth and SOA formation rates at ground level are likely to be influenced by the reduced HOM concentrations in the inversion nights. However, there are still limitations due to current experiment design, such as horizontal separation in instrument set-up, or the uncertainties from using point measurements at two heights to infer larger scale exchange. Clearly, more vertical and planar measurements of HOMs are needed to confirm the emerging picture presented here. Influence of boundary layer dynamics should be better characterized and evaluated in future field campaigns.

Acknowledgements

This work was supported by the IBAIRN project, the academy of Finland FCoE atmosphere, European commission Actris2 and Actris PPP, the European Research Council (Grant 638703-COALA), transnational access from ENVRI plus, and SMEAR II technical team. Q.Z. thanks ATM-DP (Doctoral Program in Atmospheric Sciences) graduate programs, John Crowley and Max Plank Institute in association with IBAIRN proposal, and the tofTools team for providing tools for mass spectrometry analysis. G.K.

400 acknowledges the support from the U.S. National Science Foundation (NSF-EAR-
401 1344703, NSF-AGS-1644382), the U.S. Department of Energy (DE-SC0011461), and
402 University of Helsinki for supporting a 3-month sabbatical leave at the Division of
403 Atmospheric Sciences.
404
405 Reference:
406 Aalto, P., Hämeri, K., Becker, E., Weber, R., Salm, J., Mäkelä, J. M., Hoell, C., O'dowd,
407 C. D., Hansson, H.-C., Väkevä, M., Koponen, I. K., Buzorius, G. and Kulmala, M.:
408 Physical characterization of aerosol particles during nucleation events, Tellus B Chem.
409 Phys. Meteorol., 53(4), 344–358, doi:10.3402/tellusb.v53i4.17127, 2001.
410 Alekseychik, P., Mammarella, I., Launiainen, S., Rannik, Ü. and Vesala, T.: Evolution
411 of the nocturnal decoupled layer in a pine forest canopy, Agric. For. Meteorol., 174, 15–
412 27, doi:10.1016/j.agrformet.2013.01.011, 2013.
413 Bäck, J., Aalto, J., Henriksson, M., Hakola, H., He, Q. and Boy, M.: Chemodiversity of
414 a Scots pine stand and implications for terpene air concentrations, Biogeosciences, 9(2),
415 689–702, doi:10.5194/bg-9-689-2012, 2012.
416 Berndt, T., Scholz, W., Mentler, B., Fischer, L., Herrmann, H., Kulmala, M. and Hansel,
417 A.: Accretion Product Formation from Self- and Cross-Reactions of RO_2 Radicals in
418 the Atmosphere, Angew. Chemie Int. Ed., 57(14), 3820–3824,
419 doi:10.1002/anie.201710989, 2018.
420 Bianchi, F., Tröstl, J., Junninen, H., Frege, C., Henne, S., Hoyle, C. R., Molteni, U.,
421 Herrmann, E., Adamov, A., Bukowiecki, N., Chen, X., Duplissy, J., Gysel, M., Hutterli,
422 M., Kangasluoma, J., Kontkanen, J., Kürten, A., Manninen, H. E., Münch, S., Peräkylä,
423 O., Petäjä, T., Rondo, L., Williamson, C., Weingartner, E., Curtius, J., Worsnop, D. R.,
424 Kulmala, M., Dommen, J. and Baltensperger, U.: New particle formation in the free
425 troposphere: A question of chemistry and timing., Science, 352(6289), 1109–12,
426 doi:10.1126/science.aad5456, 2016.
427 Bianchi, F., Garmash, O., He, X., Yan, C., Iyer, S., Rosendahl, I., Xu, Z., Rissanen, M.

P., Riva, M., Taipale, R., Sarnela, N., Petäjä, T., Worsnop, D. R., Kulmala, M., Ehn, M. and Junninen, H.: The role of highly oxygenated molecules (HOMs) in determining the composition of ambient ions in the boreal forest, Atmos. Chem. Phys., 17(22), 13819–13831, doi:10.5194/acp-17-13819-2017, 2017.

Chen, X., Quéléver, L. L. J., Fung, P. L., Kesti, J., Rissanen, M. P., Bäck, J., Keronen, P., Junninen, H., Petäjä, T., Kerminen, V.-M. and Kulmala, M.: Observations of ozone depletion events in a Finnish boreal forest, Atmos. Chem. Phys., 18(1), 49–63, doi:10.5194/acp-18-49-2018, 2018.

Crounse, J. D., Nielsen, L. B., Jørgensen, S., Kjaergaard, H. G. and Wennberg, P. O.: Autoxidation of Organic Compounds in the Atmosphere, J. Phys. Chem. Lett., 4(20), 3513–3520, doi:10.1021/jz4019207, 2013.

Dada, L., Paasonen, P., Nieminen, T., Mazon, S. B., Kontkanen, J., Peräkylä, O., Lehtipalo, K., Hussein, T., Petäjä, T., Kerminen, V.-M., Bäck, J. and Kulmala, M.: Long-term analysis of clear-sky new particle formation events and nonevents in Hyytiälä, Atmos. Chem. Phys, 17, 6227–6241, doi:10.5194/acp-17-6227-2017, 2017.

Eerdekens, G., Yassaa, N., Sinha, V., Aalto, P. P., Aufmhoff, H., Arnold, F., Fiedler, V., Kulmala, M. and Williams, J.: VOC measurements within a boreal forest during spring 2005: on the occurrence of elevated monoterpene concentrations during night time intense particle concentration events, Atmos. Chem. Phys., 9(21), 8331–8350, doi:10.5194/acp-9-8331-2009, 2009.

Ehn, M., Junninen, H., Petäjä, T., Kurtén, T., Kerminen, V.-M., Schobesberger, S., Manninen, H. E., Ortega, I. K., Vehkamäki, H., Kulmala, M. and Worsnop, D. R.: Composition and temporal behavior of ambient ions in the boreal forest, Atmos. Chem. Phys., 10(17), 8513–8530, doi:10.5194/acp-10-8513-2010, 2010.

Ehn, M., Kleist, E., Junninen, H., Petäjä, T., Lönn, G., Schobesberger, S., Dal Maso, M., Trimborn, A., Kulmala, M., Worsnop, D. R., Wahner, A., Wildt, J. and Mentel, T. F.: Gas phase formation of extremely oxidized pinene reaction products in chamber and ambient air, Atmos. Chem. Phys., 12(11), 5113–5127, doi:10.5194/acp-12-5113-2012,

2012.

Ehn, M., Thornton, J. A., Kleist, E., Sipilä, M., Junninen, H., Pullinen, I., Springer, M., Rubach, F., Tillmann, R., Lee, B., Lopez-Hilfiker, F., Andres, S., Acir, I.-H., Rissanen, M., Jokinen, T., Schobesberger, S., Kangasluoma, J., Kontkanen, J., Nieminen, T., Kurtén, T., Nielsen, L. B., Jørgensen, S., Kjaergaard, H. G., Canagaratna, M., Maso, M. D., Berndt, T., Petäjä, T., Wahner, A., Kerminen, V.-M., Kulmala, M., Worsnop, D. R., Wildt, J. and Mentel, T. F.: A large source of low-volatility secondary organic aerosol, Nature, 506(7489), 476–479, doi:10.1038/nature13032, 2014.

Ehn, M., Berndt, T., Wildt, J. and Mentel, T.: Highly Oxygenated Molecules from Atmospheric Autoxidation of Hydrocarbons: A Prominent Challenge for Chemical Kinetics Studies, Int. J. Chem. Kinet., 49(11), 821–831, doi:10.1002/kin.21130, 2017.

Hari, P., Nikinmaa, E., Pohja, T., Siivola, E., Bäck, J., Vesala, T. and Kulmala, M.: Station for measuring ecosystem-atmosphere relations: SMEAR, Phys. Physiol. For. Ecol., 9789400756, 471–487, doi:10.1007/978-94-007-5603-8_9, 2013.

Heinritzi, M., Simon, M., Steiner, G., Wagner, A. C., Kürten, A., Hansel, A. and Curtius, J.: Characterization of the mass-dependent transmission efficiency of a CIMS, Atmos. Meas. Tech., 9(4), 1449–1460, doi:10.5194/amt-9-1449-2016, 2016.

Jokinen, T., Sipilä, M., Junninen, H., Ehn, M., Lönn, G., Hakala, J., Petäjä, T., Mauldin, R. L., Kulmala, M. and Worsnop, D. R.: Atmospheric sulphuric acid and neutral cluster measurements using CI-APi-TOF, Atmos. Chem. Phys., 12(9), 4117–4125, doi:10.5194/acp-12-4117-2012, 2012.

Jokinen, T., Sipilä, M., Richters, S., Kerminen, V.-M., Paasonen, P., Stratmann, F., Worsnop, D., Kulmala, M., Ehn, M., Herrmann, H. and Berndt, T.: Rapid Autoxidation Forms Highly Oxidized RO_2 Radicals in the Atmosphere, Angew. Chemie Int. Ed., 53(52), 14596–14600, doi:10.1002/anie.201408566, 2014.

Jokinen, T., Kausiala, O., Garmash, O., Peräkylä, O., Junninen, H., Schobesberger, S., Yan, C., Sipilä, M. and Rissanen, M. P.: Production of highly oxidized organic compounds from ozonolysis of β-caryophyllene: laboratory and field measurements,

Boreal Env. Res, 21, 262–273, 2016.

Junninen, H., Ehn, M., Petäjä, T., Luosujärvi, L., Kotiaho, T., Kostiainen, R., Rohner, U., Gonin, M., Fuhrer, K., Kulmala, M. and Worsnop, D. R.: A high-resolution mass spectrometer to measure atmospheric ion composition, Atmos. Meas. Tech., 3(4), 1039–1053, doi:10.5194/amt-3-1039-2010, 2010.

Katul, G. G., Finnigan, J. J., Poggi, D., Leuning, R. and Belcher, S. E.: The Influence of Hilly Terrain on Canopy-Atmosphere Carbon Dioxide Exchange, Boundary-Layer Meteorol., 118(1), 189–216, doi:10.1007/s10546-005-6436-2, 2006.

Katul, G. G., Porporato, A., Shah, S. and Bou-Zeid, E.: Two phenomenological constants explain similarity laws in stably stratified turbulence, Phys. Rev. E, 89(2), 023007, doi:10.1103/PhysRevE.89.023007, 2014.

Kirkby, J., Duplissy, J., Sengupta, K., Frege, C., Gordon, H., Williamson, C., Heinritzi, M., Simon, M., Yan, C., Almeida, J., Tröstl, J., Nieminen, T., Ortega, I. K., Wagner, R., Adamov, A., Amorim, A., Bernhammer, A.-K., Bianchi, F., Breitenlechner, M., Brilke, S., Chen, X., Craven, J., Dias, A., Ehrhart, S., Flagan, R. C., Franchin, A., Fuchs, C., Guida, R., Hakala, J., Hoyle, C. R., Jokinen, T., Junninen, H., Kangasluoma, J., Kim, J., Krapf, M., Kürten, A., Laaksonen, A., Lehtipalo, K., Makhmutov, V., Mathot, S., Molteni, U., Onnela, A., Peräkylä, O., Piel, F., Petäjä, T., Praplan, A. P., Pringle, K., Rap, A., Richards, N. A. D., Riipinen, I., Rissanen, M. P., Rondo, L., Sarnela, N., Schobesberger, S., Scott, C. E., Seinfeld, J. H., Sipilä, M., Steiner, G., Stozhkov, Y., Stratmann, F., Tomé, A., Virtanen, A., Vogel, A. L., Wagner, A. C., Wagner, P. E., Weingartner, E., Wimmer, D., Winkler, P. M., Ye, P., Zhang, X., Hansel, A., Dommen, J., Donahue, N. M., Worsnop, D. R., Baltensperger, U., Kulmala, M., Carslaw, K. S. and Curtius, J.: Ion-induced nucleation of pure biogenic particles, Nature, 533(7604), 521–526, doi:10.1038/nature17953, 2016.

Kulmala, L., Launiainen, S., Pumpanen, J., Lankreijer, H., Lindroth, A., Hari, P. and Vesala, T.: H_2O and CO_2 fluxes at the floor of a boreal pine forest, Tellus, Ser. B Chem. Phys. Meteorol., 60 B(2), 167–178, doi:10.1111/j.1600-0889.2007.00327.x, 2008.

512 Kulmala, M., Dal Maso, M., Mäkelä, J. M., Pirjola, L., Väkevä, M., Aalto, P.,
513 Miikkulainen, P., Hämeri, K. and O'Dowd, C. D.: On the formation, growth and
514 composition of nucleation mode particles, Tellus, Ser. B Chem. Phys. Meteorol., 53(4),
515 479–490, doi:10.3402/tellusb.v53i4.16622, 2001.
516 Kulmala, M., Kontkanen, J., Junninen, H., Lehtipalo, K., Manninen, H. E., Nieminen,
517 T., Petäjä, T., Sipilä, M., Schobesberger, S., Rantala, P., Franchin, A., Jokinen, T.,
518 Järvinen, E., Äijälä, M., Kangasluoma, J., Hakala, J., Aalto, P. P., Paasonen, P., Mikkilä,
519 J., Vanhanen, J., Aalto, J., Hakola, H., Makkonen, U., Ruuskanen, T., Mauldin, R. L.,
520 Duplissy, J., Vehkamäki, H., Bäck, J., Kortelainen, A., Riipinen, I., Kurtén, T., Johnston,
521 M. V, Smith, J. N., Ehn, M., Mentel, T. F., Lehtinen, K. E. J., Laaksonen, A., Kerminen,
522 V.-M. and Worsnop, D. R.: Direct observations of atmospheric aerosol nucleation.,
523 Science, 339(6122), 943–6, doi:10.1126/science.1227385, 2013.
524 Kürten, A., Bergen, A., Heinritzi, M., Leiminger, M., Lorenz, V., Piel, F., Simon, M.,
525 Sitals, R., Wagner, A. C. and Curtius, J.: Observation of new particle formation and
526 measurement of sulfuric acid, ammonia, amines and highly oxidized organic molecules
527 at a rural site in central Germany, Atmos. Chem. Phys, 16, 12793–12813,
528 doi:10.5194/acp-16-12793-2016, 2016.
529 Launiainen, S., Katul, G. G., Grönholm, T. and Vesala, T.: Partitioning ozone fluxes
530 between canopy and forest floor by measurements and a multi-layer model, Agric. For.
531 Meteorol., 173, 85–99, doi:10.1016/j.agrformet.2012.12.009, 2013.
532 Lauros, J., Nilsson, E. D., Dal Maso, M. and Kulmala, M.: Contribution of mixing in
533 the ABL to new particle formation based on observations, Atmos. Chem. Phys., 7(18),
534 4781–4792, doi:10.5194/acp-7-4781-2007, 2007.
535 Mahrt, L.: Nocturnal Boundary-Layer Regimes, Boundary-Layer Meteorol., 88(2),
536 255–278, doi:10.1023/A:1001171313493, 1998.
537 Mahrt, L., Vickers, D., Nakamura, R., Soler, M. R., Sun, J., Burns, S. and Lenschow, D.
538 H.: Shallow Drainage Flows, Boundary-Layer Meteorol., 101(2), 243–260,
539 doi:10.1023/A:1019273314378, 2001.

Mammarella, I., Kolari, P., Rinne, J., Keronen, P., Pumpanen, J. and Vesala, T.: Determining the contribution of vertical advection to the net ecosystem exchange at Hyytiälä forest, Finland, Tellus B Chem. Phys. Meteorol., 59(5), 900–909, doi:10.1111/j.1600-0889.2007.00306.x, 2007.

Mentel, T. F., Springer, M., Ehn, M., Kleist, E., Pullinen, I., Kurtén, T., Rissanen, M., Wahner, A. and Wildt, J.: Formation of highly oxidized multifunctional compounds: autoxidation of peroxy radicals formed in the ozonolysis of alkenes–deduced from structure–product relationships, Atmos. Chem. Phys. Discuss., 15(2), 2791–2851, 2015.

Orlando, J. J. and Tyndall, G. S.: Laboratory studies of organic peroxy radical chemistry: an overview with emphasis on recent issues of atmospheric significance, Chem. Soc. Rev., 41(19), 6294, doi:10.1039/c2cs35166h, 2012.

Ouwersloot, H. G., Vilà-Guerau de Arellano, J., Nölscher, A. C., Krol, M. C., Ganzeveld, L. N., Breitenberger, C., Mammarella, I., Williams, J. and Lelieveld, J.: Characterization of a boreal convective boundary layer and its impact on atmospheric chemistry during HUMPPA-COPEC-2010, Atmos. Chem. Phys., 12(19), 9335–9353, doi:10.5194/acp-12-9335-2012, 2012.

Rannik, Ü., Mammarella, I., Keronen, P. and Vesala, T.: Vertical advection and nocturnal deposition of ozone over a boreal pine forest, Atmos. Chem. Phys., 9(6), 2089–2095, doi:10.5194/acp-9-2089-2009, 2009.

Rannik, Ü., Altimir, N., Mammarella, I., Bäck, J., Rinne, J., Ruuskanen, T. M., Hari, P., Vesala, T. and Kulmala, M.: Ozone deposition into a boreal forest over a decade of observations: evaluating deposition partitioning and driving variables, Atmos. Chem. Phys., 12(24), 12165–12182, doi:10.5194/acp-12-12165-2012, 2012.

Rantala, P., Taipale, R., Kajos, M. K., Patokoski, J., Ruuskanen, T. M., Rinne, J. and Aalto, J.: Continuous flux measurements of VOCs using PTR-MS — Reliability and feasibility of disjunct-eddy-covariance, surface-layer-gradient, and surface-layer-profile methods, Boreal Environ. Res., 19, 87–107, 2014.

Raupach, M. R. and Thom, A. S.: Turbulence in and above Plant Canopies, Annu. Rev.

568 Fluid Mech., 13(1), 97–129, doi:10.1146/annurev.fl.13.010181.000525, 1981.
569 Rissanen, M. P., Kurtén, T., Sipilä, M., Thornton, J. A., Kangasluoma, J., Sarnela, N.,
570 Junninen, H., Jørgensen, S., Schallhart, S., Kajos, M. K., Taipale, R., Springer, M.,
571 Mentel, T. F., Ruuskanen, T., Petäjä, T., Worsnop, D. R., Kjaergaard, H. G. and Ehn, M.:
572 The Formation of Highly Oxidized Multifunctional Products in the Ozonolysis of
573 Cyclohexene, J. Am. Chem. Soc., 136(44), 15596–15606, doi:10.1021/ja507146s, 2014.
574 Taipale, R., Ruuskanen, T. M., Rinne, J., Kajos, M. K., Hakola, H., Pohja, T. and
575 Kulmala, M.: Technical Note: Quantitative long-term measurements of VOC
576 concentrations by PTR-MS - measurement, calibration, and volume mixing ratio
577 calculation methods, Atmos. Chem. Phys., 8(22), 6681–6698, doi:10.5194/acp-8-6681-
578 2008, 2008.
579 Tröstl, J., Chuang, W. K., Gordon, H., Heinritzi, M., Yan, C., Molteni, U., Ahlm, L.,
580 Frege, C., Bianchi, F., Wagner, R., Simon, M., Lehtipalo, K., Williamson, C., Craven,
581 J. S., Duplissy, J., Adamov, A., Almeida, J., Bernhammer, A.-K., Breitenlechner, M.,
582 Brilke, S., Dias, A., Ehrhart, S., Flagan, R. C., Franchin, A., Fuchs, C., Guida, R., Gysel,
583 M., Hansel, A., Hoyle, C. R., Jokinen, T., Junninen, H., Kangasluoma, J., Keskinen, H.,
584 Kim, J., Krapf, M., Kürten, A., Laaksonen, A., Lawler, M., Leiminger, M., Mathot, S.,
585 Möhler, O., Nieminen, T., Onnela, A., Petäjä, T., Piel, F. M., Miettinen, P., Rissanen, M.
586 P., Rondo, L., Sarnela, N., Schobesberger, S., Sengupta, K., Sipilä, M., Smith, J. N.,
587 Steiner, G., Tomè, A., Virtanen, A., Wagner, A. C., Weingartner, E., Wimmer, D.,
588 Winkler, P. M., Ye, P., Carslaw, K. S., Curtius, J., Dommen, J., Kirkby, J., Kulmala, M.,
589 Riipinen, I., Worsnop, D. R., Donahue, N. M. and Baltensperger, U.: The role of low-
590 volatility organic compounds in initial particle growth in the atmosphere, Nature,
591 533(7604), 527–531, doi:10.1038/nature18271, 2016.
592 Vickers, D., Irvine, J., Martin, J. G. and Law, B. E.: Nocturnal subcanopy flow regimes
593 and missing carbon dioxide, Agric. For. Meteorol., 152(1), 101–108,
594 doi:10.1016/j.agrformet.2011.09.004, 2012.
595 Viggiano, A. A., Seeley, J. V., Mundis, P. L., Williamson, J. S. and Morris, R. A.: Rate

Constants for the Reactions of XO_3-$(H_2O)_n$ (X = C, HC, and N) and NO_3-(HNO_3)n with H_2SO_4: Implications for Atmospheric Detection of H_2SO_4, J. Phys. Chem. A, 101(44), 8275–8278, doi:10.1021/jp971768h, 1997.

Yan, C., Nie, W., Äijälä, M., Rissanen, M. P., Canagaratna, M. R., Massoli, P., Junninen, H., Jokinen, T., Sarnela, N., Häme, S. A. K., Schobesberger, S., Canonaco, F., Yao, L., Prévôt, A. S. H., Petäjä, T., Kulmala, M., Sipilä, M., Worsnop, D. R. and Ehn, M.: Source characterization of highly oxidized multifunctional compounds in a boreal forest environment using positive matrix factorization, Atmos. Chem. Phys., 16(19), 12715–12731, doi:10.5194/acp-16-12715-2016, 2016.

Zhao, J., Ortega, J., Chen, M., McMurry, P. H. and Smith, J. N.: Dependence of particle nucleation and growth on high-molecular-weight gas-phase products during ozonolysis of α-pinene, Atmos. Chem. Phys., 13(15), 7631–7644, doi:10.5194/acp-13-7631-2013, 2013.